Moroccan Journal of Chemistry
ISSN : 2351-812X

Mor. J. Chem., 2023, Volume 11, Issue 4, Page 1299-1318
https://revues.imist.ma/index.php/morjchem
https://doi.org/10.48317/IMIST.PRSM/morjchem-v11i04.43414

Application of Castor plant (Ricinus communis. L) as a green sorbent for removing cationic dyes from textile effluents

Ait Oukharaz N. [1], Lakhmiri R. [1]*, El Fargani H. [1], Eladnani I. [1], Sguillar M. [1], Albourine A. [2], Bazzi L. [3], Safi M. [4], Cherkaoui O. [5]

[1]Team of Chemical Engineering and Valorization of the Resources, Faculty of Sciences and Techniques of Tangier, Abdelmalek Essaadi University, Km 10 route de Ziaten, BP 416 Tangier, Morocco.
[2]Laboratory of Materials and Environment, Team of Coordination Chemistry, Faculty of Sciences, Ibn Zohr University, BP 8106, 80000 Agadir, Morocco.
[3]Laboratory of Industrial Engineering, Energy and Environment (LI3E), SupMTI, Rabat, Morocco.
[4]Laboratory of Physical Chemistry and Bio-Organic Chemistry, Faculty of Sciences and Techniques- Mohammedia, URAC 22 University of Hassan II Mohammedia-Casablanca, BP 146, Mohammedia, Morocco.
[5]Laboratory REMTEX, Higher School of Textile and Clothing Industries, Casablanca, Morocco.
**Corresponding author, Email address: lakhmirir@yahoo.fr*

Received *27 Sept 2023,*
Revised *26 Oct 2023,*
Accepted *28 Oct 2023*

Citation: *Ait Oukharaz N., Lakhmiri R., El Fargani H., Eladnani I., Sguillar M., Albourine A., Bazzi L., Safi M., Cherkaoui O. (2023) Application of Castor plant (Ricinus communis L.) as a green sorbent for removing cationic dyes from textile effluents., Mor. J. Chem., 11(4), 1299-1318*

Abstract: The present study reports the removal of cationic dyes from water using Castor plant byproducts (castor seed shell (CC), castor seed shell envelope (CE), and castor leaves (CF)) as low-cost and ecofriendly materials. The different parts of the castor plant were characterized using various techniques such as FTIR, X-Ray diffraction, SEM and EDX analysis. Dye adsorption experiments were conducted in a batch reactor to study the kinetics, thermodynamics, and equilibrium of the adsorption process. The adsorption was strongly described by Langmuir isotherm, and followed the pseudo second-order-kinetic model. The thermodynamic parameters indicate that the adsorption in this case is an exothermic, spontaneous and physical process. The results showed that all the castor plant materials had a much higher uptake capacity for the Toluidine Blue (TB) dye compared to Yellow X-GL 200% (YX-GL) one, reaching maximum adsorption capacities above 1107.69 $mg.g^{-1}$ for BT and 109.02 $mg.g^{-1}$ for YX-GL. The desorption study showed that different Castor plant based-adsorbents could be reused multiple times (at last 6 times) without losing their adsorption performance. Overall, the experimental outcomes demonstrated that the Castor plant byproducts may be considered as efficient and reusable alternative adsorbents for the treatment of dye-contaminated effluents.

Keywords: Green material; Castor plant; Adsorption; Cationic dyes; Yellow X-GL 200%; Toluidine Blue.

Abbreviations:
CC: castor seed shell
CE: castor seed shell envelope
CF: castor leaves
EDXA: energy dispersive X-ray spectrometry
ETAD, Ecological and Toxicological Association of Dye manufacturers
LD_{50}: lethal doses
TB: Toluidine Blue
SEM: scanning electron microscope

1. Introduction

Industrial effluents are the main source of dye contaminants in water resources. Considering the industrialization and population growth, the water demand has increased in recent years. The amount

of wastewater has also increased significantly due to the effluents and emissions discharged from various factories. Textile dyes are a particular concern, as they produce a lot of pollution, in both qualitative and quantitative terms. Complex effluents from dye manufacturers often have variable physicochemical characteristics, making their treatment challenging (N'daye *et al.*, 2023; Smahi 2017). The presence of dyes in water decrease the photosynthesis process and dissolved oxygen levels, resulting detrimental effects on ecosystems (Khandare and Govindwar 2015; Saratale *et al.* 2011; Rais *et al.* 2008). A study by the ETAD, (Ecological and Toxicological Association of Dye manufacturers) evaluated over 4,000 dyes, of which 90% were found to be relatively harmless, with lethal doses (LD_{50}) greater than 2 $g.kg^{-1}$. Cationic dyes had the highest LD_{50} values (Anliker 1979). There are various methods for removing these colored substances, such as complexation (Elhoudi *et al.* 2021), ion exchange, chemical precipitation, reverse osmosis, solvent extraction, and adsorption (Rashid *et al.* 2021). Furthermore, in developing countries, dye removal methods are often not feasible due to technical limitations and financial constraints. Therefore, there is a need for simple and affordable dye removal methods that can be used in these countries. Precipitation-filtration is a relatively inexpensive dye removal method, but it is complex to implement. Ion exchange and membrane separation are simpler methods, but the cost of ion exchange resins is a barrier to their widespread use in developing countries (Batouti *et al.* 2016). The complexation method is also an effective and selective method for removing dyes (Elhoudi *et al.* 2021). However, it can produce waste and be less effective than other methods for removing dark colored dyes. Adsorption is cost-effective, environmentally friendly, and can be reproduced on a large scale and in developing countries (Vakili *et al.* 2019). Researchers are increasingly focused on developing effective and affordable adsorbents from waste agricultural materials (Oladoja *et al.* 2008) such as Castor plant (Ricinus communis L). This is because Castor plants are a readily available and inexpensive source of materials that can be used to remove pollutants from water (Rodríguez-Yáñez 2019).

On the other hand, preventing corrosion is essential to extend the lifespan of hydraulic equipment. The effectiveness of the water treatment can be affected by the condition of hydraulic equipment, hence the importance of using organic corrosion inhibitors as mentioned by Bouchtart *et al.* 2020. These organic inhibitors will extend the life of water treatment equipment and consequently preserve their performance for water treatment.

The Castor plant has been used as a source of several biosorbents. Castor seed shells have been studied for their ability to remove basic dyes (Sah *et al.* 2022; Silva *et al.* 2021; Oladoja *et al.* 2008), and castor leaves have also been the subject of a study to adsorb heavy metals (Martins *et al.* 2013, Makeswari and Santhi 2014).

In the present study, various Castor plant by-products such as seed shell (CC), the envelope of the castor seed shell (CE), the combination of CC and CE (CEC), and Castor leaves (CF) were thoroughly characterized (FTIR, X-Ray diffraction, SEM and EDX analysis) and used as adsorbents to remove Yellow X-GL 200% (YX-GL) and Toluidine Blue (TB) dyes from wastewater. The uptake capacity was investigated as a function of different operation parameters including pH, adsorption time, adsorbent dose, dye concentration and temperature. The actual data were analyzed using isotherm, kinetic and thermodynamic models. Furthermore, the regeneration experiments were performed in order to evaluate the recycling performance of these biosorbents. On the whole, the current research work aims to valorize an agricultural waste as a promising alternative to other chemically synthesized adsorbents.

2. Materials and methods

2.1 Materials

All the reagents used in this work were of analytical grade (i.e., Hydrochloric acid (HCl) and sodium hydroxide (NaOH). YX-GL and TB were provided from Laboratory REMTEX (Morocco). The Castor plant by-products such as CC, CE, CEC and CF were collected from different locations in the Tangier region of Morocco **(Figure 1)**. The biosorbents were grown, separated, rinsed with distilled water, dried at 60°C, crushed, and sieved to a size of 100µm. Distilled water was used to prepare all of the stock solutions.

Figure 1. Photographs of **a)** Castor tree **b)** Castor leaves **c)** Castor seed shell and **d)** envelope of the castor seed shell.

2.2 Characterization of materials

A scanning electron microscope (SEM) and energy dispersive X-ray spectrometry (EDXA) were used to visualize the morphologies of the bio-adsorbents. The EDXA can be used to qualitatively detect and localize the elements present in CC, CE, CEC and CF. Fourier transform infrared spectroscopy (FTIR – JASCO FT/IR-410)) was used to identify the functional groups present on the surfaces of the four biomaterials in the wavenumber range from 400 cm^{-1} to 4000 cm^{-1}. The structures of the materials were then determined using X-ray diffraction (XRD). The point of zero charge (pH_{ZPC}) was also measured, as it provides an indication of the charge of the material's surfaces as a function of pH. The pH_{zpc} of CC, CE, CEC and CF were determined using the method defined by Fiol and Villaescusa 2009.

2.3. Dye adsorption batch experiments

The adsorption of YX-GL and TB dyes by four materials (CC, CE, CEC, and CF) was investigated under different conditions including adsorbent dose, contact time, concentration, pH, and temperature. The pH was adjusted with 0.1M NaOH or 0.1M HCl. The dye concentrations ranged from 10 to 600 $mg.L^{-1}$. In all experiments, 15 mg of biomaterial was added into 30 mL of dye solution. The mixtures were stirred continuously at 250 rpm and kept at a temperature of 30°C. After adsorption, the solutions

were centrifuged and filtered. To quantify the equilibrium concentrations of YX-GL and TB, the filtrate solution was analyzed using a JASCO V-360 UV spectrophotometer at maximum wavelengths of λ_{YX-GL} = 435 nm and λ_{TB} = 625 nm. The adsorbed dye concentration was measured using UV spectrometry. The adsorbed amount (Q_e) was calculated using **Eqn. 1**, and the dye removal percentage was calculated using **Eqn. 2**:

$$Q_e = \frac{V}{m} \times (C_0 - C_e) \qquad \textbf{Eqn.1}$$

$$\%R = 100\frac{C_0 - C_e}{C_0} \qquad \textbf{Eqn.2}$$

- Q_e (mg. g^{-1}): the amount of adsorbed dye at equilibrium;
- V: the volume of solution (L);
- C_0: the initial dye concentration (mg.L^{-1});
- C_e: the dye concentration at equilibrium (mg. L^{-1});
- m: the weight (g) of the adsorbent used.

2.4. Kinetic modelling

The pseudo-first-order and pseudo-second-order kinetic models are used to describe different processes that take place during the adsorption of YX-GL and TB onto CC, CE, CEC and CF. The pseudo-first-order model is generally expressed by **Eqn. 3**.

$$Q_t = Q_e(1 - e^{-k_1 t}) \qquad \textbf{Eqn.3}$$

where Q_t (mg. g^{-1}) and Q_e (mg. g^{-1}) denote the amounts of dye adsorbed at time t and at equilibrium, respectively. k_1 (h^{-1}) is the pseudo-first-order constant.

Pseudo-second-order model is defined by **Eqn. 4**:

$$Q_t = \frac{k_2 Q_e^2 t}{1 + k_2 Q_e t} \qquad \textbf{Eqn.4}$$

where k_2 (g.mg^{-1}.h^{-1}) represents the adsorption rate constant of pseudo-second-order.

2.5. Isotherm models

To understand how adsorbents bind to adsorbates, the adsorption equilibrium data were analyzed using isotherm models. The Langmuir, Freundlich, Temkin, and Dubinin-Radushkevich (D-R) models are the most commonly used. The Langmuir model **(Eqn. 5)** (Dadda, 2012) assumes that adsorption takes place on a homogeneous surface with the same affinity for all binding sites. This results in the formation of a monolayer of adsorbate (Sherlala *et al.* 2019).

$$\frac{1}{Q_e} = \left(\frac{1}{K_L . Q_m}\right)\frac{1}{C_e} + \frac{1}{Q_m} \qquad \textbf{Eqn.5}$$

where Q_e is the quantity of pollutant adsorbed per unit of adsorbent (mg. g^{-1}), C_e (mg. L^{-1}) denotes the concentration of YX-GL and TB. Q_m (mg. g^{-1}) represents the maximum adsorption capacity, K_L (L. mg^{-1}) is the Langmuir constant related to energy adsorption and represents the affinity with adsorbent and adsorbate.

The most important function of the Langmuir isotherm is the dimensionless separation factor (R_L), which can be used to assess the quality of the fit of the model to the experimental data. The R_L is calculated using the **Eqn. 6.**

$$R_L = \frac{1}{1+K_L.C_0}$$ **Eqn.*6***

where C_0 is the initial concentration (mg. L^{-1}) of YX-GL and TB.

The type of adsorption isotherm can be determined by the value of the dimensionless separation factor (R_L). If $0 < R_L < 1$, the isotherm is favorable. If $R_L > 1$, the isotherm is unfavorable. If $R_L = 1$, the isotherm is linear. If $R_L = 0$, the isotherm is irreversible.

The Freundlich isotherm model **(Eqn. 7)** hypothesizes that the surface energy of the adsorbent is heterogeneous. This means that the adsorption heat is not uniformly distributed on the surface of the adsorbent. As a result, the amount of adsorbate adsorbed is not limited to the formation of a monolayer on the adsorbent surface.

$$lnQ_e = lnK_f + \frac{1}{n_f} lnC_e$$ **Eqn.*7***

where K_f and n_f denote the relative adsorption capacity and the dependence degree of adsorption on the adsorbate equilibrium concentration, respectively.

The Temkin isotherm model assumes that the adsorption heat of all molecules in the layer decreases linearly with the coverage. This is due to the indirect interactions between the adsorbate and adsorbent molecules (Rajahmundry *et al.* 2021). The Temkin isotherm is different from the Freundlich isotherm, which assumes that the adsorption heat decreases logarithmically with the coverage. The Temkin equation is represented by **Eqn. 8**.

$$Q_{e=Bln\left(\frac{RT}{b_t}\right)+Bln(C_e)}$$ **Eqn.*8***

where B represents the constant related to the heat of sorption (J. mol^{-1}). b_T is the Temkin isotherm constant. R denotes the gas constant (8.314 J.mol^{-1}. K^{-1}). T is the temperature of the system at 298K.

The Dubinin-Radushkevich (D-R) isotherm model is based on the assumption that the surface of the adsorbent is heterogeneous and adsorption is related to the volume of adsorbent pores (Mozaffari Majd *et al.* 2022). The D-R isotherm model also assumes that the free adsorption enthalpy is related to the degree of filling of the pores. This means that the energy required to adsorb a molecule onto the surface of the adsorbent is different for various pores (Mobarak *et al.* 2019). The D-R equation is represented by **Eqn. 9.**

$$ln(Q_e) = ln(Q_m) - K_D\xi^2$$ **Eqn.9**

where K_D is Dubinin constant (mol^2. kJ^{-2}) and ξ represents the potential of Polanyi (ξ = RT ln $(1 + \frac{1}{C_e})$.

The free energy of adsorption (E_{DR}) is often used to distinguish between physical and chemical adsorption. It is calculated using **Eqn. 10**, which is a thermodynamic equation that takes into account the enthalpy and entropy of adsorption (Dadda, 2012).

$$E_{DR} = \frac{1}{\sqrt{2B_{DR}}}$$ **Eqn.*10***

2.6. Thermodynamics functions

The thermodynamic data of the adsorption process can provide insights into its nature and spontaneity (Ridha and Webley 2010, Auta and Hameed 2012). The three integral thermodynamics functions are represented by **Eqns. 11 and 12** and namely the free energy change ($\Delta G°$), enthalpy change ($\Delta H°$) and entropy change ($\Delta S°$), can be used to understand the thermodynamic behaviour of the adsorption process.

$$\Delta G° = -RTlnK_c \qquad \textbf{Eqn.}\textit{11}$$

$$lnK_c = -\frac{\Delta H°}{R}\frac{1}{T} + \frac{\Delta S°}{R} \qquad \textbf{Eqn.}\textit{12}$$

where R is the Universal gas constant (8.314 J. mol^{-l}. K^{-1}). T represents the absolute temperature (K). K_c denotes the distribution coefficient.

3. Results and Discussion

3.1 Characterization of biosorbent materials

Fourier transform infrared (FTIR) spectroscopy is a powerful technique to identify and characterize chemical compounds. FTIR spectra of CC, CE, CEC, and CF materials exhibit significant bands **(Figure 2)** associated with the functional moieties present in these materials. **Table 1** represents the significant bands for the four materials. The vibrations between 3280 cm^{-1} and 3400 cm^{-1} indicate the presence of phenol and alcohols. The absorption bands between 2850 cm^{-1} and 2930 cm^{-1} related to the C-H vibrations in the CH_2 or CH_3 groups. The C=O stretching vibrations are detected between 1700 cm^{-1} and 1750 cm^{-1}, indicating the presence of ester, ketones, aldehydes and carboxylic acids for CC and CEC. The absorption peaks between 1600cm^{-1} and 1640 cm^{-1} represent C=C stretching vibrations in alkenes and aromatics. C-H deformation vibrations between 1340 cm^{-1} and 1420 cm^{-1} indicate the presence of alkanes. Amine groups were identified between 1000 cm^{-1} et 1270 cm^{-1}, which correspond to C-N and N-H stretching vibrations. Absorption peaks located between 550 cm^{-1} and 650 cm^{-1} indicate the presence of C-C vibrations, suggesting the presence of polycyclic and substituted aromatic groups (Martins *et al.* 2013, Makeswari and Santhi 2014).

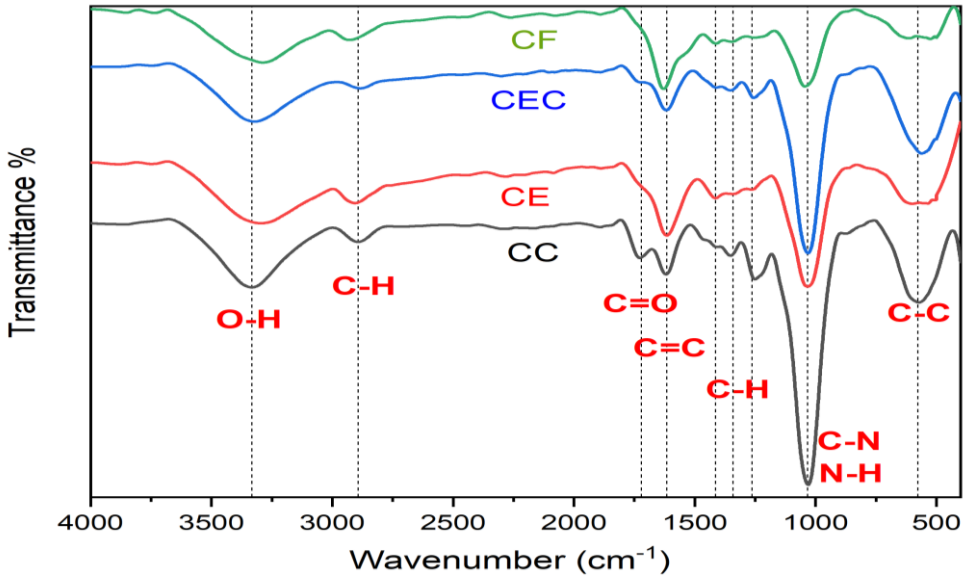

Figure 2. FTIR spectrum of CC, CE, CEC, and CF.

Figure 3 displays the SEM images of the four materials CC, CE, CEC and CF. These images show the morphology of each biosorbent. It is clear that the four materials have a fibrous structure. For CC and CF, it can be seen that the fibers are arranged in parallel. These beams of fibers are separated by spaces that can serve as adsorption sites. On the other hand, for the EC, the SEM shows a fibrous agglomeration containing pores. For the image of the CEC, we observe the two types of morphology, the fibrous beams and the fibrous agglomeration. Energy-dispersive X-ray spectroscopy (EDS) analysis **(Figure 4)** was used to determine the elemental composition of CC, CE, CEC, and CF particles. **Figure 4** shows that the four biomaterials contain primarily carbon (C), oxygen (O) and

nitrogen (N). Furthermore, the presence of other minor elements such as silicon (Si), aluminum (Al), sulfur (S), and phosphorus (P) was detected, which could be attributed to the mineral soil impurities. **Table 2** shows the % weight elements of CC, CE, CEC, and CF. The presence of these elements in plant structure was also confirmed by (Dara *et al.* 2021).

Table 1. Principal absorption bands of CC, CE, CEC and CF.

Absorption bands (cm^{-1})				Attributions
CC	CE	CEC	CF	
3332	3296	3321	3287	Stretching vibrations of OH on phenols and in side chains (-CH-OH) and (-CH_2-OH)
2856	2906	2880	2929	Stretching vibration of C-H bonds in the CH_2 or CH_3 groups
1741	-	1753	-	Stretching vibrations of C=O (ester – ketone – aldehyedes – carbocylic acids)
1618	1616	1617	1629	Stretching vibration of C=C (alkene - aromatic)
1411	1414	1410	1413	Stretching vibrations of C-H (alkane)
1349	1341	1348	1346	
1251	1264	1258	1253	Stretching vibrations of C-N and N-H (amine groups)
1031	1033	1031	1044	
572	587	562	612	Stretching vibrations of C-C (Polycyclics and aromatic)

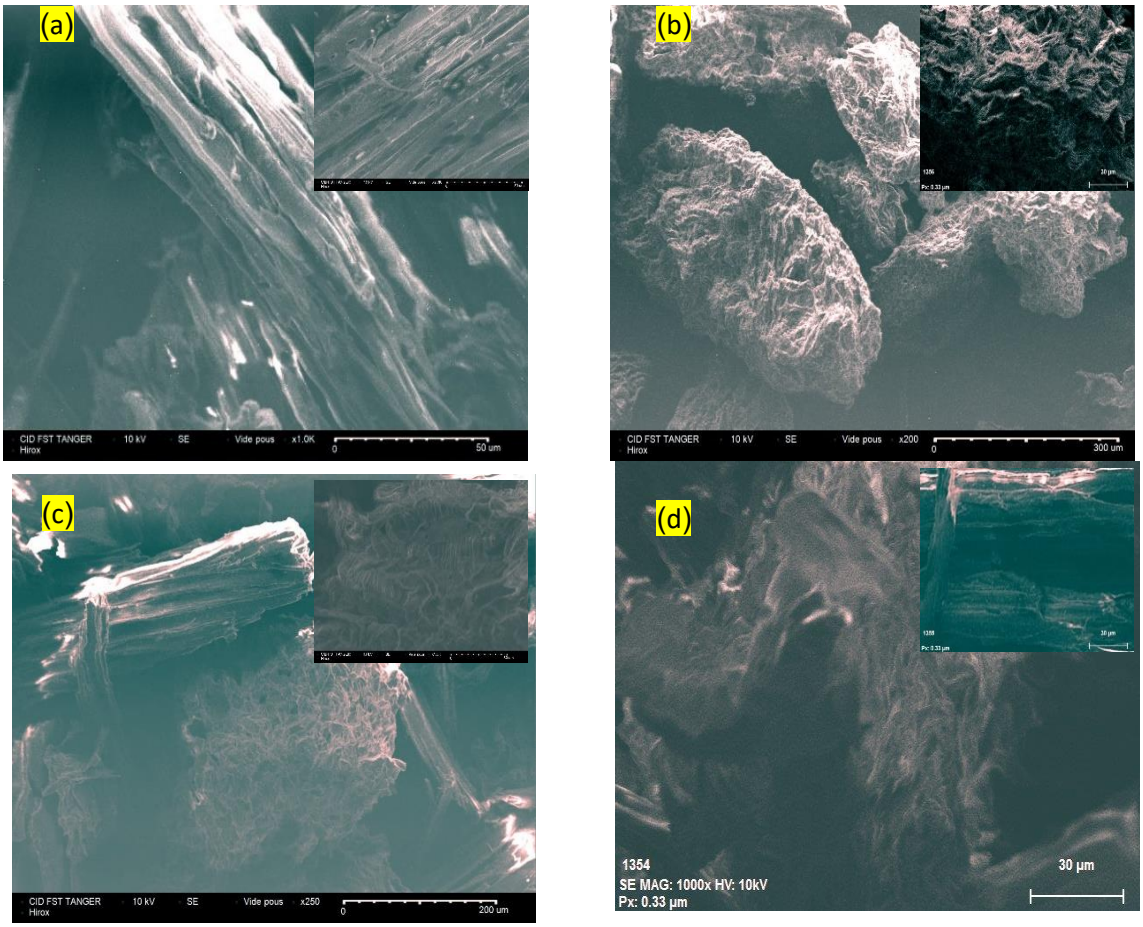

Figure 3. SEM images of **(a)** CC, **(b)** CE, **(c)** CEC and **(d)** CF.

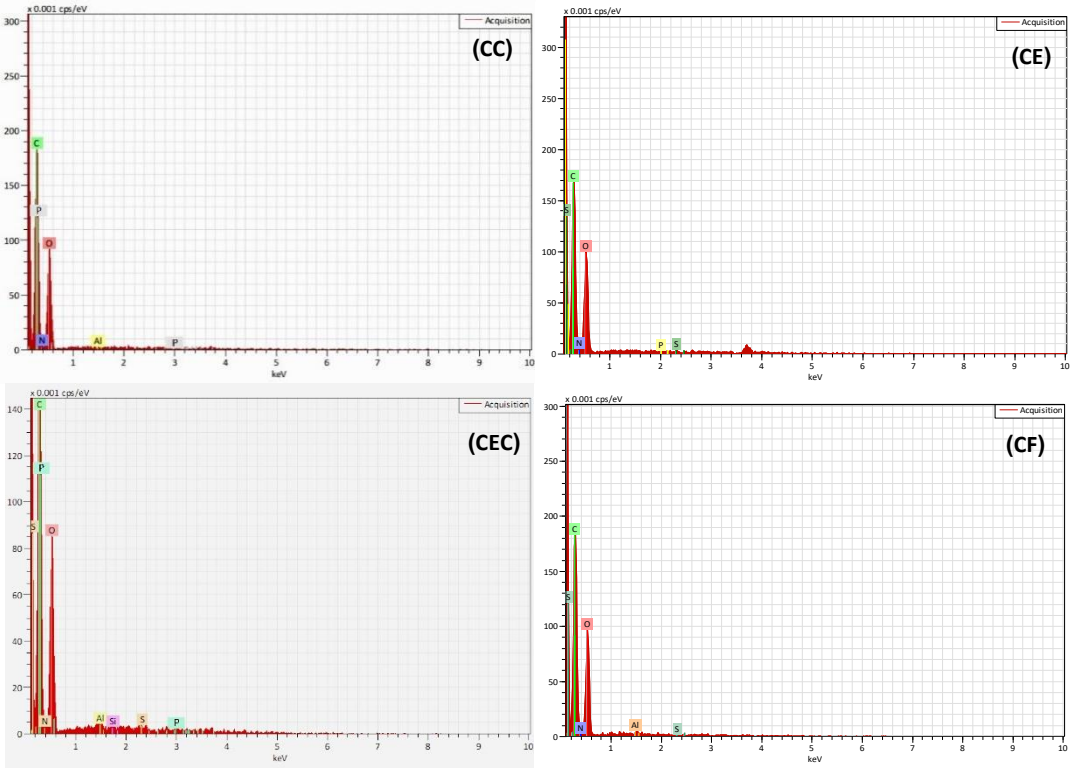

Figure 4. EDX diffractograms of CC, CE, CEC, and CF.

Table 2. Element weight percentages of CC, CE, CEC, and CF.

Element	Weight%			
	CC	CE	CEC	CF
Carbon	71.82	67.06	74.34	69.88
Oxygen	25.74	24.68	23.29	18.69
Nitrogen	2.38	8.20	2.11	6.30
Aluminum	0.01	-	0.09	0.05
Phosphorus	0.05	0.01	0.08	-
Sulfur	-	0.06	0.03	0.02
silicon	-	-	0.07	-

Figure 5 shows the X-ray diffraction patterns of CC, CE, CEC, and CF biosorbents. The characteristic 2θ peaks of each material are 21.74° and 15.89° for CC, 21.20° and 15.09 for CE, 22.007 and 15.63° for CEC and finally 20.47° and 15.29° for CF **(Table.3)**. These diffraction peaks may be attributed to (002) and (101) planes of cellulose (Essekri *et al.* 2023). Furthermore, the presence of broad peaks in the spectra of the Castor plant byproducts indicated that these materials were mostly amorphous (Makeswari and Santhi 2014).

Table 3. Characteristic peaks of CC, CE, CEC, and CF.

	CC		CE		CEC		CF	
2 Θ	21.74°	15.89°	21.20°	15.09°	22.007°	15.63°	20.47°	15.29°

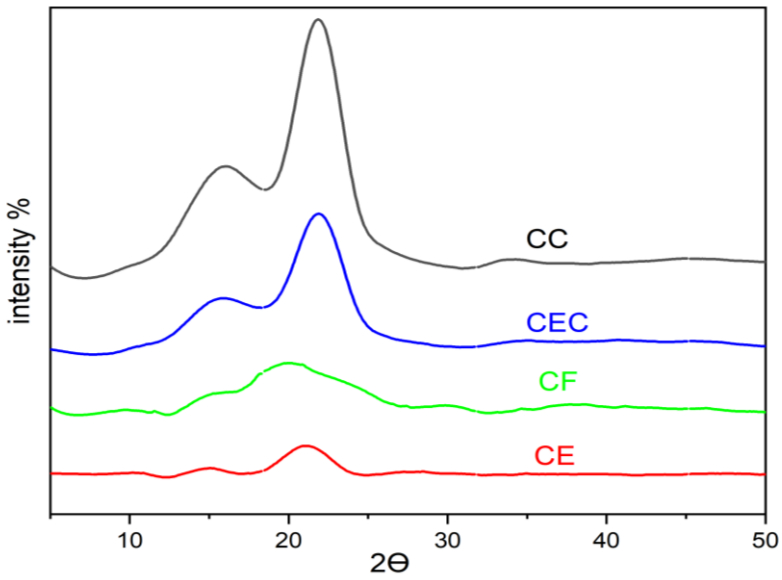

Figure 5. X-ray diffractograms of CC, CE, CEC, and CF.

According to Jing Xu mentioned (Xu *et al.* 2018), the measurement of the zero point of charge (ZPC) is important because it can affect the electrostatic adsorption in an aqueous medium. We can see that the pH_{ZPC} curve of each material intersects the x-axis at one point **(Figure 6, Table 4)**. At this point, the charge of the material is zero. Above this value, the material is negatively charged, and below this value, it is positively charged (Zhi and Zaini 2017). This means that the cationic adsorption of dyes (YX-GL and TB) is more favorable at pH values above the pH_{ZPC} for each material.

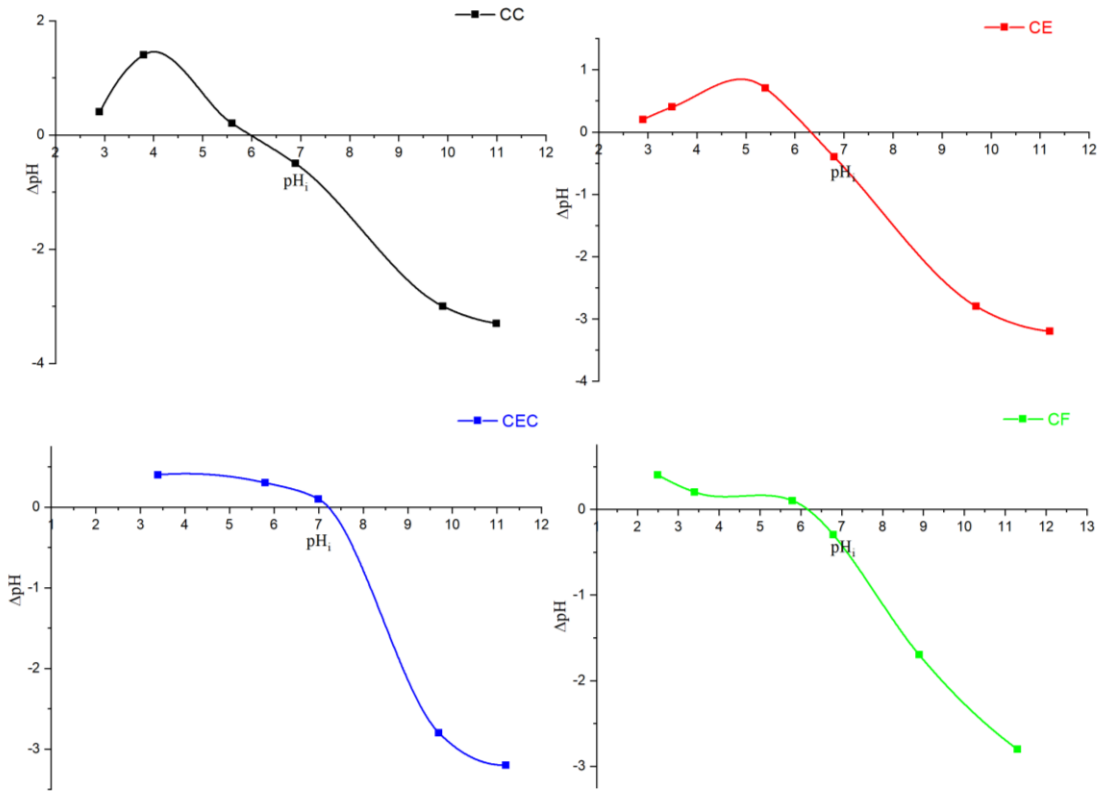

Figure 6. Determining the pH_{ZPC} values of CC, CE, CEC, and CF.

Table 4. pH_{ZPC} values of CC, CE, CEC, and CF.

	CC	CE	CEC	CF
pH_{ZPC}	6	6.4	7.2	6.2

3.2. Adsorption study

3.2.1. Effect of contact time

The sorption of YX-GL and TB by Castor plant byproducts was studied as a function of contact time **(Figure 7)**. The adsorption efficiency of TB increased rapidly during the first 20 minutes and reached a plateau after 30 minutes. This suggests that the system reaches equilibrium within 30 minutes and increasing the contact time beyond this point has no significant effect on the adsorption efficiency. This is probably because there are many sorption sites available at the beginning of the dye-adsorbent contact (Al Rmalli *et al.* 2008). For the adsorption of YX-GL, we can see that the removal efficiency increases sharply in the first 30 minutes, then continues at a steady rate until it reaches equilibrium at 60 minutes. This is because all of the available adsorption sites on the surface of the material have been filled by the YX-GL molecules at this point. However, for CF adsorption, it takes slightly more time than the other materials (CC, CE, and CEC) to reach equilibrium. This could be attributed to the difficulty of accessing the adsorption sites owing to the material's morphology (section 3.2).

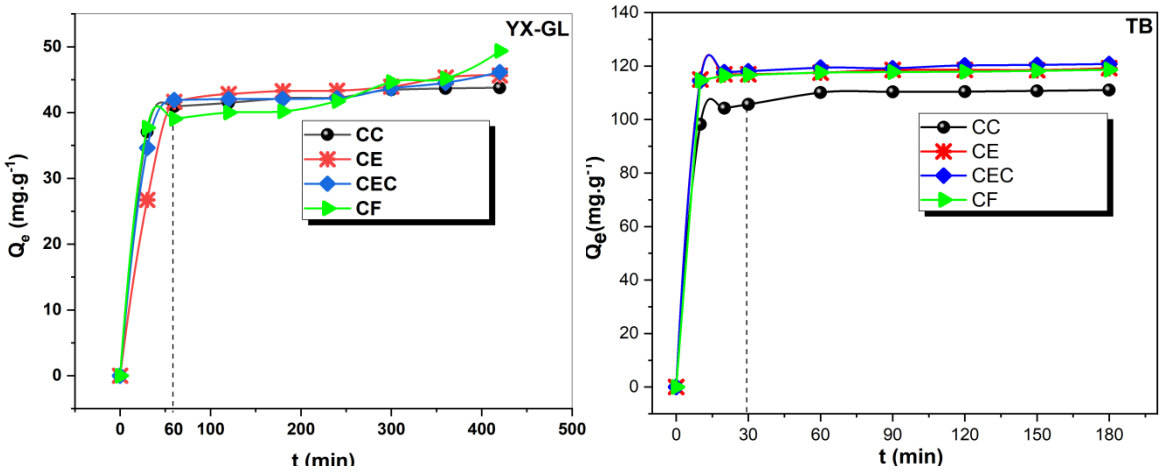

Figure 7. Effect of contact time on the adsorption of YX-GL, TB; (Conditions : [$C_{i\ YX\text{-}GL}$] = 50 mg.L^{-1}, m $_{YX\text{-}GL}$ = 20 mg, V $_{YX\text{-}GL}$= 30 mL, pH $_{YX\text{-}GL}$ = 7, T $_{YX\text{-}GL}$ = 30°C; [$C_{i\ TB}$] = 50mg.L^{-1}, m TB = 12 mg, V $_{TB}$ = 30 mL, pH $_{TB}$ = 7, T $_{TB}$ = 30°C)

3.2.2. Effect of adsorbent dose

The effect of the amount of adsorbent used on the adsorption of YX-GL and TB by Castor plant byproducts is shown in **Figures 8 and 9**, respectively. This effect is measured by the amount of YX-GL or TB adsorbed per gram of adsorbent (Q_e) and the percentage of YX-GL or TB removed from the solution (R%). The amount of adsorbent used varied from 1.5 to 100 mg for YX-GL and from 4 to 40 mg for TB. As shown in **Figures 8 and 9**, and noted in **Table 5**, the removal efficiency of YX-GL and TB by CC, CE, CEC, and CF increased with the amount of adsorbent used. This is because increasing the amount of adsorbent provides more active sites for adsorption (Aarab *et al.*, 2020). However, the amount of dye adsorbed by the four materials decreases as the adsorbent dose increases **(Table 5)**. This decrease is primarily due to the filling of adsorption sites, but it can also be explained by the possibility of aggregation of CC, CE, CEC, and CF particles, resulting in a decrease in their total surface area (Taimur *et al.*, 2017, Mahmoodi *et al.* 2011). It is known that the adsorbed quantity Q_e is more important than the adsorption rate (R%) for quantifying adsorption. This is because the adsorption rate

considering the mass of the adsorbent used, which can lead to erroneous comparisons between different adsorption systems. For this reason, the optimal dose for the elimination of the two dyes was determined graphically. This is the point of intersection of the two curves (R% and Q_e). Therefore, a mass of 15mg was chosen to carry out the next adsorption runs.

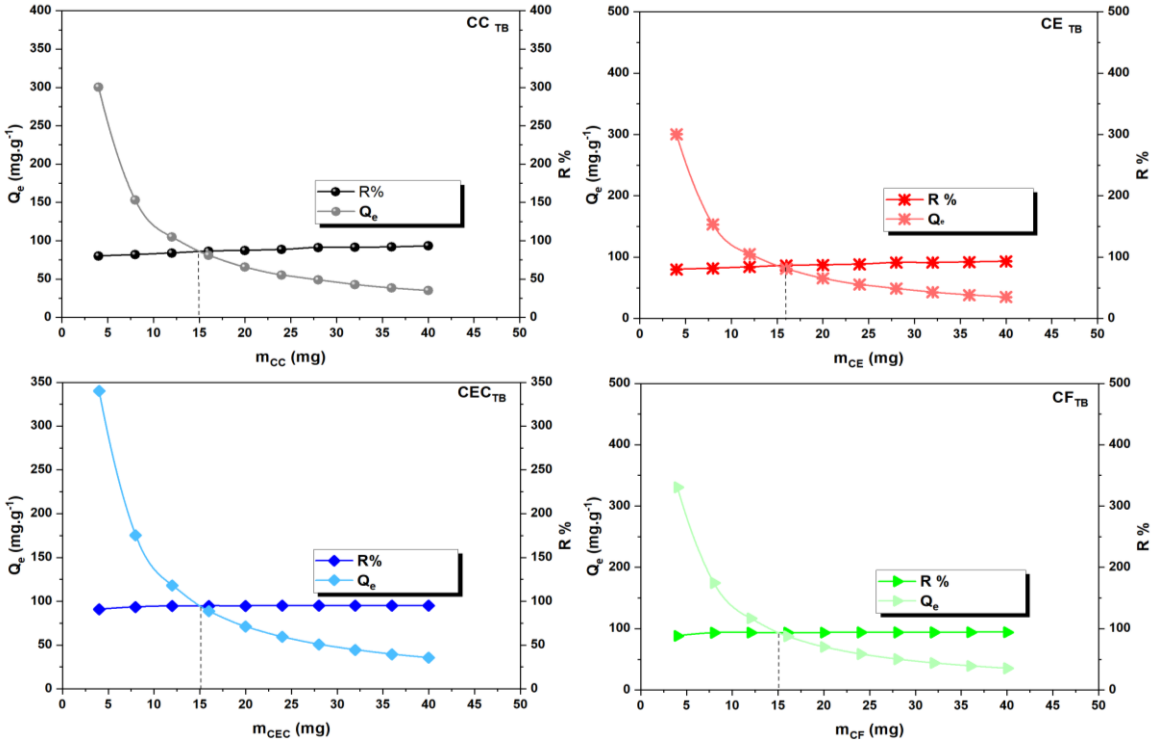

Figure 8. Effect of adsorbent dose of CC, CE, CEC, and CF on the adsorption of TB (Conditions: [Ci TB] = 50m g.L-1, tc TB = 30 min, V TB= 30 mL, pH TB = 7, T TB = 30°C).

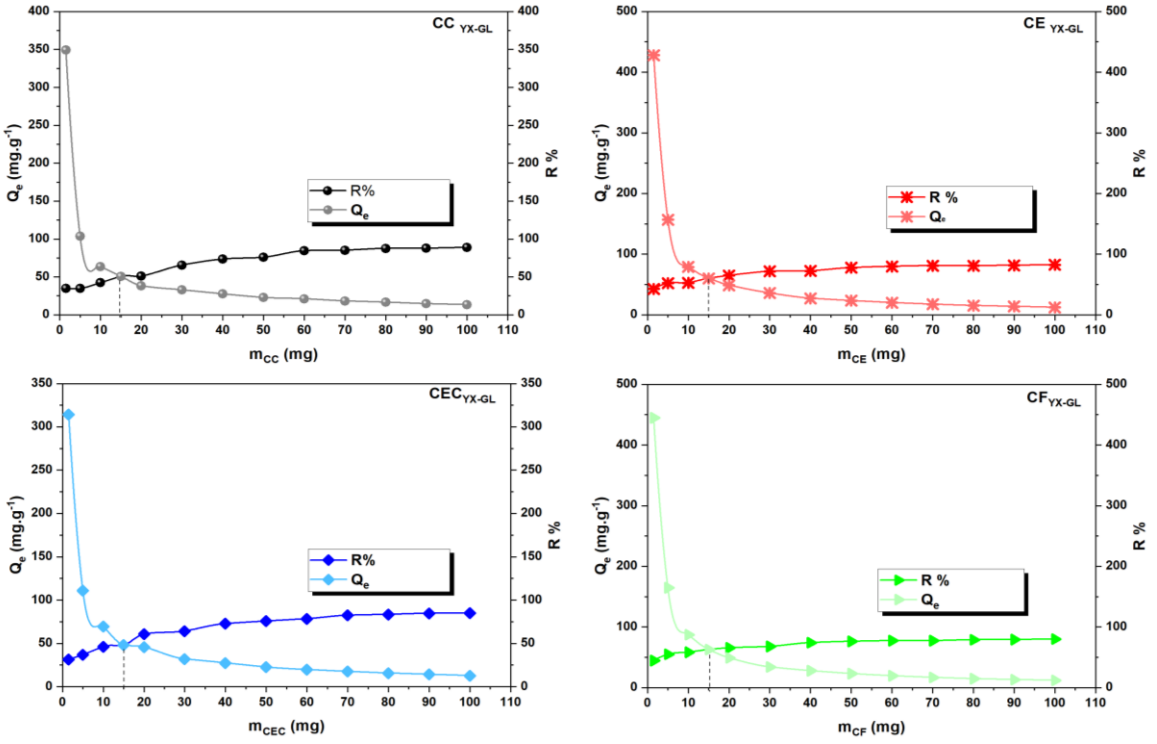

Figure 9. Effect of adsorbent dose of CC, CE, CEC, and CF on the adsorption of YX-GL (Conditions: [$C_{i\ YX-GL}$] = 50 mg.L^{-1}, $t_{c\ YX-GL}$ = 60 min, V_{YX-GL}= 30 mL, pH_{YX-GL} = 7, T_{YX-GL} = 30°C).

Table 5. The variations in R% and Q_e of the two dyes at the beginning and end of the mass adsorption study.

		CC		CE		CEC		CF	
		From	To	From	To	From	To	From	To
R%	YX-GL	34.90	88.79	42.79	82.37	31.39	84.88	44.46	80.02
	TB	80.09	93.10	80.09	93.10	90.67	94.98	88.09	94.21
Q_e (mg.g^{-1})	YX-GL	349.01	13.31	427.97	12.35	313.94	12.73	444.60	12.003
	TB	300.34	34.91	300.34	34.91	340.03	35.61	330.34	35.33

3.2.3. Effect of pH

The pH of the solution is one of the most important variables on the adsorption process, as it is responsible for the protonation and deprotonation of the surface functional groups in an aqueous solution. **Figure 10** shows the variation in the amount adsorbed as a function of the solution's pH. It is clear that the adsorption capacity increases with increasing pH. At pH < 6, the adsorption phenomenon is very weak, whereas beyond this value the adsorption becomes more important. This can be explained by the charge of the material surface. As the study of the pH_{ZPC} of the four biosorbents showed, at a value of $pH_{ZPC.CC}$ > 6, $pH_{ZPC.CE}$ > 6.4, $pH_{ZPC.CEC}$ > 7.2 and $pH_{ZPC.CC}$ > 6.2, the charge of the material is negative (deprotonated functional groups), which favors the adsorption of cationic dyes (YX-GL and TB) that have a positive charge. In contrast, at pH < pH_{ZPC}, the positive charge density at the surface of the four biomaterials increases (protonation of functional groups), which leads to a lower removal performance of the studied cationic dyes (Noroozi *et al.* 2008). Therefore, it can be concluded that the electrostatic interactions play a prominent role in the adsorption mechanism.

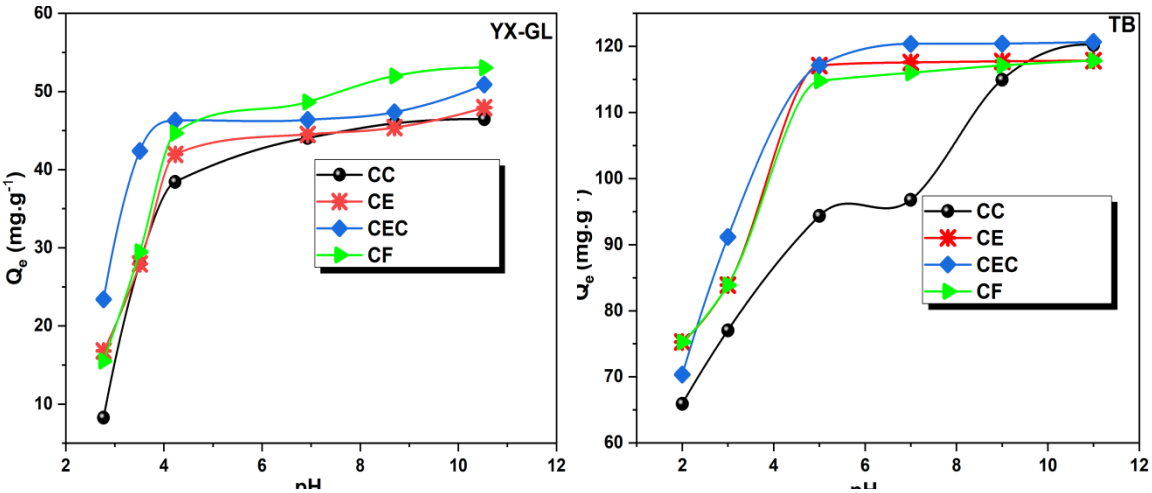

Figure 10. Effect of pH on the adsorption of YX-GL and TB (Conditions: [$C_{i\ YX\text{-}GL}$] = 50 mg.L^{-1}, m $_{YX\text{-}GL}$ = 15 mg, V $_{YX\text{-}GL}$= 30 mL, $t_{c\ YX\text{-}GL}$ = 60 min, T $_{YX\text{-}GL}$ = 25°C; [$C_{i\ TB}$] = 50 mg.L^{-1}, m $_{TB}$ = 15 mg, V $_{TB}$ = 30 mL, $t_{c\ TB}$ = 30 min, T $_{TB}$ = 30°C).

3.2.4. Effect of initial concentration

The adsorption capacities of CC, CE, CEC, and CF biosorbent towards YX-GL and TB dyes were studied by changing dye concentration at 30°C, as shown in **Figure 11**. The results showed that the adsorption capacities of the Castor plant byproducts increased gradually with increasing dye concentration. The adsorption capacity of TB was significantly higher than that of YX-GL. The increase in the amount adsorbed as a function of the initial concentration of the two dyes may be attributed to the increase in the driving force (diffusion) due to the concentration gradient (Pellera *et al.* 2012). Other interpretations attribute this phenomenon to the increase in the probability of collision between the dyes and the surfaces of the adsorbent materials (Noeline *et al.* 2005, Wong *et al.* 2003).

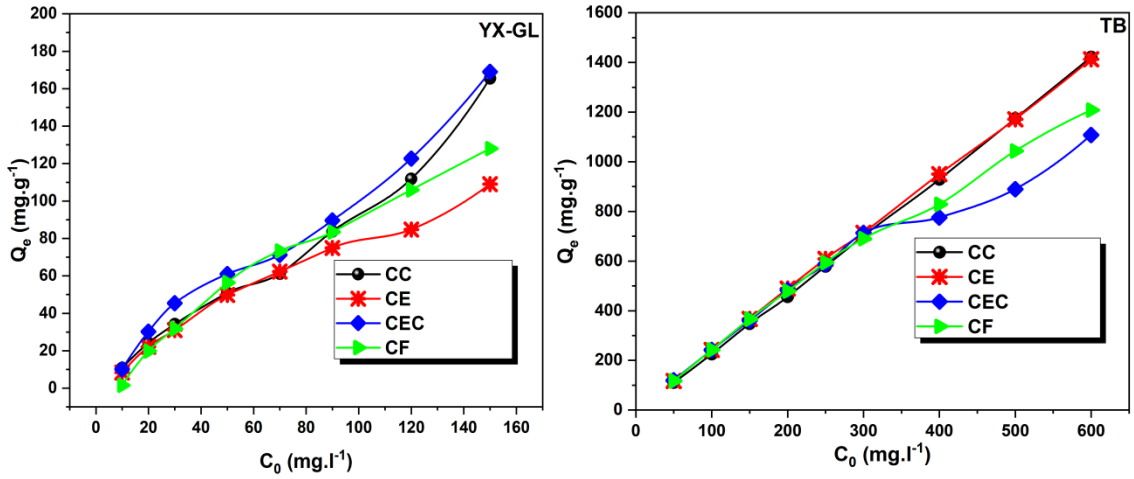

Figure 11. Effect of initial concentration on the adsorption of YX-GL and TB (Conditions: m $_{YX-GL}$ = 15mg, V $_{YX-GL}$= 30mL, $t_{c\ YX-GL}$ =60 min, T $_{YX-GL}$ = 30°C, pH $_{YX-GL}$ = 8; m $_{TB}$ = 15mg, V $_{TB}$ = 30mL, $t_{c\ TB}$ = 30 min, T $_{TB}$ = 30°C, pH $_{TB}$ = 8).

In order to understand how the YX-GL and TB dyes are distributed on the surfaces of the CC, CE, CEC, and CF adsorbents, the Langmuir, Freundlich, Temkin, and Dubinin-Radushkevich (D-R) adsorption models were used. The fit parameters of the four models and the maximum adsorption capacities for YX-GL and TB are shown in **Table 6.**

Table 6. Adsorption isotherm parameters of YX-GL onto CC, CE, CEC, and CF.

Model	Parameters	YX-GL			
		CC	CE	CEC	CF
Langmuir	Q_{max} (mg.g^{-1})	181.81	149.25	169.49	188.67
	K_L (L.mg^{-1})	0.0185	0.019	0.048	0.019
	R_L	044-0.92	7×10^{-5} – 0.001	0.19- 0.76	0.99-1
	R^2	0.9637	0.9951	0.9305	0.9855
Freundlich	K_f (mg.g^{-1})	3.3618	5.6310	6.61	9.383
	n_f	1.166	1.546	1.37	1.727
	$1/n_f$	0.857	0.646	0.729	0.579
	R^2	0.9568	0.987	0.871	0.9744
Temkin	B (J.mol^{-1})	0.0171	0.0294	0.0191	0.0195
	b_T	144960.18	84313.57	129781.105	127118.93
	A_T (L.g^{-1})	6.417×10^{50}	5.18×10^{24}	8.11×10^{34}	1.177×10^{46}
	R^2	0.7839	0.9689	0.8067	0.9814
D-R	Q_{max} (mg.g^{-1})	78.46	71.34	101.22	115.26
	K_D	9×10^{-6}	$2\times10^{—5}$	8×10^{-6}	5×10^{-5}
	E (kJ.mol^{-1})	74.5355	158.11	250	100
	R^2	0.7828	0.9006	0.7885	0.8441
$Q_{max.exp}$ (mg.g^{-1})		165.46	109.02	168.98	127.95

Table 7. Adsorption isotherm parameters of TB onto CC, CE, CEC, and CF.

Model	Parameters	TB			
		CC	CE	CEC	CF
Langmuir	Q_{max} ($mg.g^{-1}$)	1333.33	1428.57	1111.11	1250
	K_L ($L.mg^{-1}$)	0.0125	0.1129	0.0873	0.0563
	R_L	0.88 - 1	0.58 – 1	0.67 - 1	0.73 - 1
	R^2	0.9637	0.9574	0.9646	0.9488
Freundlich	K_f ($mg.g^{-1}$)	2.519	22340	163.61	143.093
	n_f	1.166	2.0437	2.786	2.178
	$1/n_f$	0.857	0.4893	0.358	0.459
	R^2	0.9568	0.9568	0.8028	0.8176
Temkin	B ($J.mol^{-1}$)	0.0014	0.0023	0.0049	0.0039
	b_T	1770505	1077747.43	505881.449	635594.641
	A_T ($L.g^{-1}$)	4.18×10^{76}	1.256×10^{80}	3.03×10^{48}	2.58×10^{35}
	R^2	0.8448	0.9282	0.9282	0.9448
D-R	Q_{max} ($mg.g^{-1}$)	930.107	1078.47	714.79	843.36
	K_D	2×10^{-5}	3×10^{-6}	2×10^{-6}	3×10^{-6}
	E ($kJ.mol^{-1}$)	158.11	408.24	500	408.248
	R^2	0.8293	0.848	0.8589	0.8367
$Q_{max.exp}$ ($mg.g^{-1}$)		1421.38	1413.076	1107.69	1208.07

Table 6 and 7 summarize the constants of the Langmuir, Freundlich, Temkin, and Dubinin-Radushkevich adsorption models for the adsorption of YX-GL and TB dyes on the biomaterials CC, CE, CEC, and CF. The Langmuir model is the most appropriate to describe the adsorption of both dyes on the four materials. The correlation coefficient (R^2) values of the Langmuir model are close to 1, indicating that the adsorption can be considered as a monolayer coverage of YX-GL and TB on a homogeneous surface of the biomaterials (Fargani *et al.* 2017). It is assumed that the active sites have the same affinity for adsorption, such that no further adsorption can occur once the sites are occupied, and no interaction between adsorbed molecules (Fargani *et al.* 2017). In addition, the maximum adsorption capacity (Q_{max}) determined using the Langmuir isotherm is in close proximity to the experimental value ($Q_{max.exp}$). Also the values of $1/n_f$ less than 1 show that there is an affinity between the biomaterials and the dyes (Aarab *et al.* 2019). Values of R_L are between 0 and 1, suggesting that the adsorption is favorable and reversible.

3.2.5. Thermodynamic study

The study of thermodynamics **(Figure 12)** is essential for understanding the behavior of matter and energy. It provides a framework for predicting how systems will behave under different conditions. That is why a study of the effect of temperature was conducted by changing the temperature from 30 to 70°C. Thermodynamic parameters such as standard free energy (ΔG°), standard enthalpy (ΔH°), and standard entropy (ΔS°) were determined using equations given in Section 2.6. As observed in **Table 7**, the negative values of ΔH° and ΔG° indicate that the adsorption is exothermic and spontaneous (Kali *et al.* 2022). The negative value of ΔS° indicates that the adsorption reduces the

disorder of the dye-biosorbent systems (Akazdam *et al.* 2019) during the adsorption process. In addition, the examination of the standard enthalpy values ($\Delta H° < 40$ kJ.mol^{-1}) shows that the adsorption of YX-GL and TB onto CC, CE, CEC, and CF is a physisorption process (Aarfane *et al.* 2014).

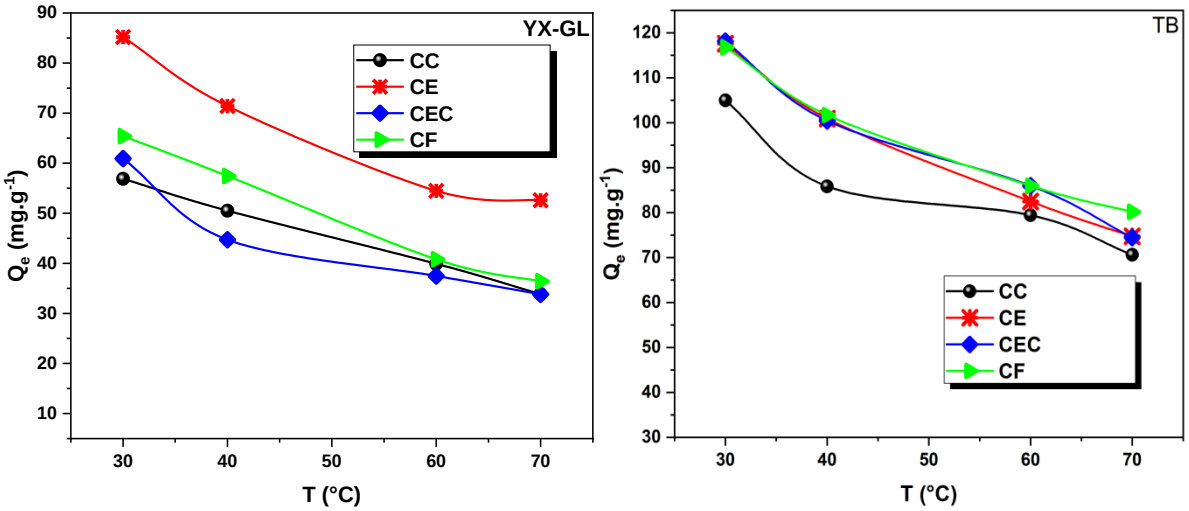

Figure 12. Effect of temperature on the adsorption of YX-GL and TB (Conditions: [$C_{i\ YX\text{-}GL}$] = 50 mg.L^{-1}, m $_{YX\text{-}GL}$ = 15 mg, V $_{YX\text{-}GL}$= 30 mL, $t_{c\ YX\text{-}GL}$ = 60 min, pH $_{YX\text{-}GL}$ = 8; [$C_{i\ TB}$] = 50mg.L^{-1}, m $_{TB}$ = 15 mg, V $_{TB}$ = 30 mL, $t_{c\ TB}$ = 30 min, pH $_{TB}$ = 8).

Table 8. Thermodynamics parameters for adsorption of YX-GL and TB.

		$\Delta H°$(kJ.mol^{-1})	$\Delta S°$(J.mol^{-1}.K^{-1})	$\Delta G°$ (kJ.mol^{-1})			
				303.15 K	313.15 K	333.15 K	343.15 K
YX-GL	CC	-3.643	-5.961	-2.444	-1.858	-0.785	-.0065
	CE	-35.112	-97.024	-6.156	-4.189	-2.418	-2.751
	CEC	-23.124	-68.079	-2.866	-1.252	-0.502	-0.061
	CF	-31.003	-90.780	-3.351	-2.585	-0.888	-0.385
TB	CC	-26.347	-67.355	-6.483	-4.431	-4.076	-3.359
	CE	-38.015	-130.396	-9.271	-6.119	-4.375	-3.745
	CEC	-24.225	-130.687	-9.473	-6.055	-4.728	-3.719
	CF	-31.212	-111.889	-9.006	-6.226	-4.275	-4.274

3.5.6. Kinetic study

Kinetic studies are essential for understanding the behavior of chemical reactions. They provide information about the rate, and the mechanism of the reaction, as well as the factors that could affect the rate of reaction. **Table 9** gives the results of the kinetic analysis for both dyes. By comparing the R^2 values of the pseudo-first-order and pseudo-second-order models, we can say that the pseudo-first-order model is less appropriate. Additionally, the calculated value of Q_e (the amount of adsorbate adsorbed at equilibrium) from the pseudo-first-order model is significantly different from the experimentally determined value (Q_{exp}). In contrast, the pseudo-second-order kinetic model better describes the adsorption of YX-GL and TB on CC, CE, CEC, and CF ($R^2 > 0.988$ for YX-GL and $R^2 = 1$ for TB). Additionally, the experimentally Q_{exp} values for the adsorption of both dyes are in excellent agreement with the Q_e values calculated from the pseudo-second-order kinetic model.

Table 9. Values of the kinetic constants for the adsorption of YX-GL and TB onto CC, CE, CEC, and CF.

		Q_{exp} (mg. g^{-1})	Pseudo-1st-order $Q_t = Q_e(1 - e^{-K_1 t})$			Pseudo-2nd-odrer $Q_t = \frac{k_2 Q_e^2 t}{1 + k_2 Q_e t}$		
			$Q_{e,1}$ (mg.g^{-1})	k_1 (min^{-1})	R^2	$Q_{e,2}$ (mg.g^{-1})	k_2 (g.mg^{-1}.min^{-1})	R^2
YX-GL	CC	43.76	8.98	0.011	0.890	44.44	0.003	0.999
	CE	45.62	12.73	0.0089	0.783	46.94	0.0013	0.998
	CEC	46.13	8.49	0.0043	0.762	46.29	0.0016	0.997
	CF	65.82	17.98	0.0031	0.906	66.66	0.0006	0.988
TB	CC	111	10.45	0.0264	0.903	112.36	0.0062	1
	CE	119.19	3.413	0.0131	0.845	212.76	0.0047	1
	CEC	120.76	5.418	0.0812	0.926	156.25	0.0064	1
	CF	118.65	3.22	0.0135	0.914	227.27	0.0044	1

3.3. Reusability of CC, CE, CEC, and CF

In practical applications, it is important for adsorbents to be stable and reusable. This means that they should be able to withstand repeated use without losing their ability to adsorb pollutants. To test the reusability of the four biomaterials (CC, CE, CEC, and CF), six adsorption/desorption cycles were performed. After each cycle, the adsorbent was regenerated with 0.1 M HCl. The results **(Figure 13)** showed that there was a slight decrease in efficiency for both dyes over the six cycles. This decrease is maybe due to the loss of biomaterial and the breakdown of polymer chains during the regeneration process. However, the overall decrease in efficiency was small, indicating that the Castor plant byproducts used in this study exhibited excellent reusability and can be used for practical applications.

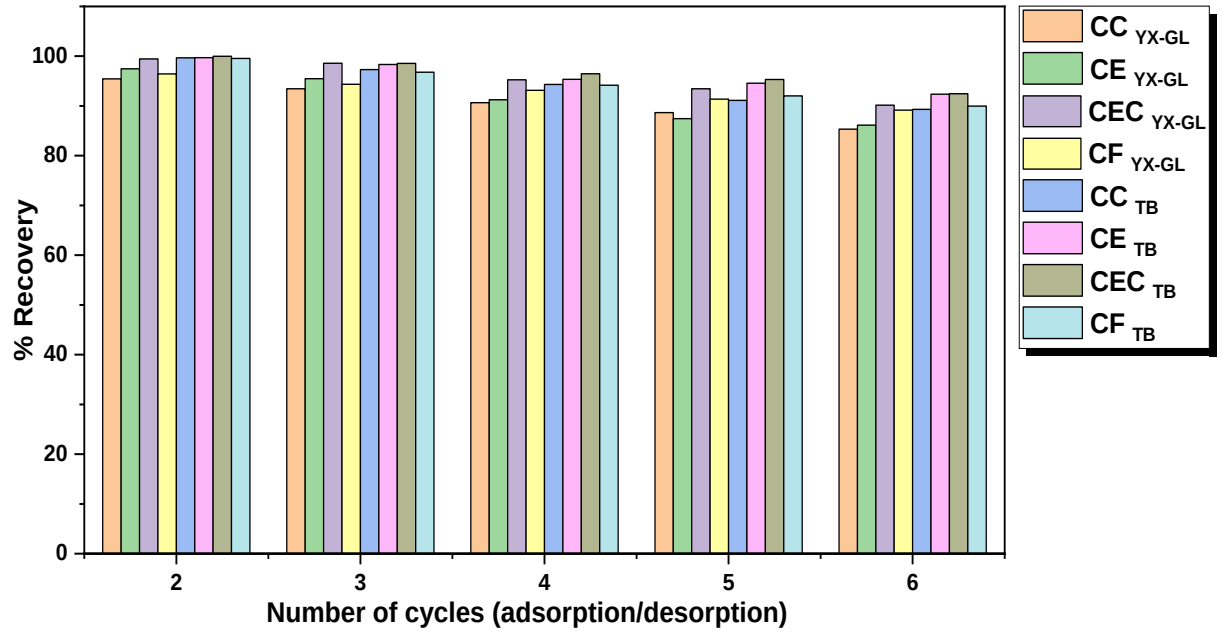

Figure 13. Reusability of CC, CE, CEC, and CF over six cycles (Conditions: $m_{YX\text{-}GL} = m_{TB} = 15$ mg , [YX-GL] = [TB] = 50 mg.l^{-1}, pH = 8, T = 30°C, $t_{cYX\text{-}GL} = 60$ min, $t_{cTB} = 30$ min).

4. Conclusion

The present study investigated the use of four biomaterials (CC, CE, CEC, and CF) derived from the castor plant as adsorbents for removing two cationic dyes YX-GL and TB from aqueous solutions. The biomaterials were characterized using various techniques. As a result, the biomaterials possessed an amorphous and fibrillar structure. The adsorption process was optimized by studying the effects of different conditions such as contact time, adsorbent dose, temperature, initial dye concentration, and pH. The results showed that the optimal adsorbent dose was 15 mg and the best adsorption capacity was achieved in an alkaline medium (pH > 7). The adsorption mechanism is mainly governed by the electrostatic attractions. The studied biomaterials have a high adsorption capacity for the dyes YX-GL and TB ($Q_{max}(CC_{YX\text{-}GL})$ = 165.46 mg.g^{-1}, $Q_{max}(CE_{YX\text{-}GL})$ = 109.02 mg.g^{-1}, $Q_{max}(CEC_{YX\text{-}GL})$ = 168.98 mg.g^{-1}, $Q_{max}(CF_{YX\text{-}GL})$ = 127.95 mg.g^{-1}, $Q_{max}(CC_{TB})$= 1421.38 mg.g^{-1}, $Q_{max}(CE_{TB})$ = 1413.07 mg.g^{-1}, $Q_{max}(CEC_{TB})$ = 1107.69 mg. g^{-1}, $Q_{max}(CF_{TB})$ = 1208.07 mg.g^{-1}). Thermodynamic parameters revealed that the adsorption was exothermic, spontaneous and physical process. The adsorption kinetic was better described by the pseudo-second-order model. Desorption studies showed that the four biomaterials had good reusability and excellent adsorption capacity even after six regeneration cycles. This study showed that waste from the castor shell plant can be used as a low-cost, eco-friendly and effective adsorbent to remove the two cationic dyes YX-GL and TB from textile wastewater, thereby reducing both agricultural waste and wastewater pollution caused by textile dyes.

Disclosure statement: *Conflict of Interest:* The authors declare that there are no conflicts of interest.
Compliance with Ethical Standards: This article does not contain any studies involving human or animal subjects.

References

Aaddouz M., Azzaoui K., Akartasse N., Mejdoubi E., Hammouti B., Taleb M., Sabbahi R., Alshahateet S.F. (2023). Removal of Methylene Blue from aqueous solution by adsorption onto hydroxyapatite nanoparticles, *Journal of Molecular Structure*, 1288, 135807, https://doi.org/10.1016/j.molstruc.2023.135807

Aarab N., Laabd M., Eljazouli H., Lakhmiri R., Kabli H., Albourine A. (2019). Experimental and DFT Studies of the Removal of Pharmaceutical Metronidazole from Water Using Polypyrrole. *International Journal of Industrial Chemistry*, 10 (3), 269–79. https://doi.org/10.1007/s40090-019-0190-7

Aarab N., Hsini A., Essekri A., Laabd M., Lakhmiri R., Albourine A. (2020 Removal of an emerging pharmaceutical pollutant (metronidazole) using PPY-PANi copolymer: Kinetics, equilibrium and DFT identification of adsorption mechanism, *Groundwater for Sustainable Development*, 11, 100416, ISSN 2352-801X, https://doi.org/10.1016/j.gsd.2020.100416

Aarfane A., Salhi A., El Krati M., Tahiri S., Monkade M., Lhadi, E.K.and Bensitel M. (2014). Etude cinétique et thermodynamique de l'adsorption des colorants Red195 et Bleu de méthylène en milieu aqueux sur les cendres volantes et les mâchefers (Kinetic and thermodynamic study of the adsorption of Red195 and Methylene blue dyes on fly ash and bottom ash in aqueous medium). *Journal of Materials and Environmental Science*, *5*(6), 1927-1939.

Akdazama, S., Chafi, W. Yassine M., et Gouricha, B. (2019). A comparative study for removal of methylene blue by NaOH treated and raw eggshells. *Moroccan Journal of Chemistry*, 7(2), 300-313. https://doi.org/10.48317/IMIST.PRSM/morjchem-v7i2.14014

Al Rmalli Shaban W., Abdella A. Dahmani, Mohamed M. Abuein, and Amar A. Gleza. (2008). Biosorption of Mercury from Aqueous Solutions by Powdered Leaves of Castor Tree (Ricinus Communis L.). *Journal of Hazardous Materials*, 152 (3), 955–59. https://doi.org/10.1016/j.jhazmat.2007.07.111.

Anliker, R. (1979). Ecotoxicology of Dyestuffs—A Joint Effort by Industry. *Ecotoxicology and Environmental Safety*, 3 (1), 59–74. https://doi.org/10.1016/0147-6513(79)90060-5.

Dada A.O., Olalekan A.P., Olatunya A. M., Dada O.J.I.J.C. (2012) Langmuir, Freundlich, Temkin and Dubinin–Radushkevich Isotherms Studies of Equilibrium Sorption of Zn^{2+} Unto Phosphoric Acid Modified Rice Husk. *IOSR Journal of Applied Chemistry*, 3 (1), 38–45. https://doi.org/10.9790/5736-0313845.

Auta M., and Hameed B.H. (2012) Modified Mesoporous Clay Adsorbent for Adsorption Isotherm and Kinetics of Methylene Blue. *Chemical Engineering Journal*, 198, 219–227. doi:10.1016/j.cej.2012.05.075.

Batouti M.El, Ahmed M.M., Salam S.M. (2016) Adsorption of Toxic Ni (II) From Aqueous Solution By Activated Carbon. *Moroccan Journal of Chemistry*, 4(4), 1130-1143 doi:10.48317/IMIST.PRSM/morjchem-v4i4.6431.

Bouchtart A., Rguiti M., EL Mouaden K., Albourine A., Chaouiki A., Bazzi L., Chetouani A. (2020) Mild Steel Corrosion Inhibition by Some Heteroatom Organic Compounds in Acetic Acid Medium. *Moroccan Journal of Chemistry*, 8 (4), 982-993. https://doi.org/10.48317/IMIST.PRSM/morjchem-v8i4.20562

Dara J.E., Omenyi S. N., and Nwigbo S. C. (2021). Potentials of Castor Seed Shell as a Reinforcement in Aluminum Matrix Composite Development. *UNIZIK Journal of Engineering and Applied Sciences* 19 (1), 400–408.

Elhoudi M., Aarab N., Laabd M., Lakhmiri R., Bazzi L., Albourine A. (2021) Quantum Chemical Approach (DFT) of the Binary Complexation of Hg(II) with L-Canavanine and L-Arginine. *Moroccan Journal of Chemistry*, 9(3), 406–15. https://doi.org/doi.org/10.48317/IMIST.PRSM/morjchem-v9i3.28145.

Elhoudi, M., Hsini, A., El Houdi, M., Lakhmiri, R., & Albourine, A. (2021). A Theoretical Investigation of Complexation for Pyrimidine Bases with Hg^{2+} and Cd^{2+} by DFT Method. *Nanotechnology for Environmental Engineering*, 6 (2), 35. https://doi.org/10.1007/s41204-021-00128-x.

Essekri, A., Laabd, M., Fatni, A., Addi, A. A., Lakhmiri, R., & Albourine, A. (2023). The Use of Raw and Modified Acacia Leaves for Adsorptive Removal of Crystal Violet from Water. *Chemical Engineering Research and Design*, 190, 143–56. https://doi.org/10.1016/j.cherd.2022.12.010.

El Fargani, H., Lakhmiri, R., Albourine, A., Safi, M., & Cherkaoui, O. (2017). Removal of Reactive Yellow 160 from Industrial Wastewater onto Modified Sand (Sand of Larache City Beach. Morocco). *Chemical and Process Engineering Research*, 52, 24-36.

El Fargani, H., Lakhmiri, R., Aitoukharaz, N., Albourine, A., Safi, M., & Cherkaoui, O. (2017). Removal of Reactive Yellow 135 from Wastewaterof Textile Industry onto Chitosan Extracted by Hydrothermo-Chemical Method. *Chemical and Materials Research*, 9 (10), 21–29.

Fiol, N., & Villaescusa, I. (2009). Determination of Sorbent Point Zero Charge: Usefulness in Sorption Studies. *Environmental Chemistry Letters*, 7 (1), 79–84. https://doi.org/10.1007/s10311-008-0139-0.

Kali A. A., Dehmani Y., Loulidi I., Amar A., Jabri M., El-Kord A., Boukhlifi F. (2022). Study of the Adsorption Properties of an Almond Shell in the Elimination of Methylene Blue in an Aquatic. *Moroccan Journal of Chemistry*, 10 (3), 509-522. https://doi.org/10.48317/IMIST.PRSM/MORJCHEM-V10I3.33140

Khandare, Rahul V., and Sanjay P. Govindwar. (2015). Phytoremediation of Textile Dyes and Effluents: Current Scenario and Future Prospects. *Biotechnology Advances*, 33 (8), 1697–1714. https://doi.org/10.1016/j.biotechadv.2015.09.003.

Mahmoodi, N. M., Salehi, R., Arami, M., & Bahrami, H. (2011). Dye Removal from Colored Textile Wastewater Using Chitosan in Binary Systems. *Desalination*, 267 (1), 64–72. https://doi.org/10.1016/j.desal.2010.09.007.

Makeswari, M., and T. Santhi. (2014). Use of Ricinus Communis Leaves as a Low-Cost Adsorbent for Removal of Cu(II) Ions from Aqueous Solution'. *Research on Chemical Intermediates*, 40 (3), 1157–77. https://doi.org/10.1007/s11164-013-1029-z.

Martins, A. E., Pereira, M. S., Jorgetto, A. O., Martines, M. A., Silva, R. I., Saeki, M. J., & Castro, G. R. (2013). The Reactive Surface of Castor Leaf [Ricinus Communis L.] Powder as a Green Adsorbent for the Removal of Heavy Metals from Natural River Water. *Applied Surface Science*, 276, 24–30. https://doi.org/10.1016/j.apsusc.2013.02.096

Mobarak, M., Mohamed, E. A., Selim, A. Q., Eissa, M. F., & Seliem, M. K. (2019). Experimental Results and Theoretical Statistical Modeling of Malachite Green Adsorption onto MCM–41 Silica/Rice Husk Composite Modified by Beta Radiation. *Journal of Molecular Liquids*, 273, 68–82. https://doi.org/10.1016/j.molliq.2018.09.132.

Majd, M. M., Kordzadeh-Kermani, V., Ghalandari, V., Askari, A., & Sillanpää, M. (2022). Adsorption Isotherm Models: A Comprehensive and Systematic Review (2010−2020). *Science of The Total Environment*, 812, 151334. https://doi.org/10.1016/j.scitotenv.2021.151334.

N'diaye A.D.., Kankou M.S.A, Hammouti B., Nandiyanto A.B.D., Al Husaeni D.F. (2023) A review of biomaterial as an adsorbent: From the bibliometric literature review, the definition of dyes and adsorbent, the adsorption phenomena and isotherm models, factors affecting the adsorption process, to the use of typha species waste as adsorbent, *Communications in Science and Technology* 7(2), 140-153

Noeline, B. F., Manohar, D. M., & Anirudhan, T. S. (2005). Kinetic and Equilibrium Modelling of Lead(II) Sorption from Water and Wastewater by Polymerized Banana Stem in a Batch Reactor. *Separation and Purification Technology*, 45 (2), 131–40. https://doi.org/10.1016/j.seppur.2005.03.004.

Noroozi, B., Sorial, G. A., Bahrami, H., & Arami, M. (2008). Adsorption of Binary Mixtures of Cationic Dyes. *Dyes and Pigments*, 76 (3), 784–91. https://doi.org/10.1016/j.dyepig.2007.02.003.

Oladoja, N. A., Aboluwoye, C. O., Oladimeji, Y. B., Ashogbon, A. O., & Otemuyiwa, I. O. (2008). Studies on Castor Seed Shell as a Sorbent in Basic Dye Contaminated Wastewater Remediation. *Desalination*, 227 (1–3), 190–203. https://doi.org/10.1016/j.desal.2007.06.025.

Pellera, F. M., Giannis, A., Kalderis, D., Anastasiadou, K., Stegmann, R., Wang, J. Y., & Gidarakos, E. (2012). Adsorption of Cu(II) Ions from Aqueous Solutions on Biochars Prepared from Agricultural by-Products. *Journal of Environmental Management*, 96 (1), 35–42. https://doi.org/10.1016/j.jenvman.2011.10.010.

Rais Z., Taleb M., Sfaira M., Filali Baba M., Hammouti B., Maghnouj J., Nejjar R., Hadji M. (2008), Decolouration of textile's effluents discoloration by adsorption in static reactor and in dynamic reactor on the phosphocalcic apatites, *Phys. Chem. News*, 38, 106-111

Rajahmundry, G. K., Garlapati, C., Kumar, P. S., Alwi, R. S., & Vo, D. V. N. (2021). Statistical Analysis of Adsorption Isotherm Models and Its Appropriate Selection. *Chemosphere*, 276, 130176. https://doi.org/10.1016/j.chemosphere.2021.130176.

Rashid, R., Shafiq, I., Akhter, P., Iqbal, M. J., & Hussain, M. (2021). A State-of-the-Art Review on Wastewater Treatment Techniques: The Effectiveness of Adsorption Method. *Environmental Science and Pollution Research*, 28 (8), 9050–66. https://doi.org/10.1007/s11356-021-12395-x.

Ridha, F. N., & Webley, P. A. (2010). Entropic Effects and Isosteric Heats of Nitrogen and Carbon Dioxide Adsorption on Chabazite Zeolites. *Microporous and Mesoporous Materials*, 132 (1–2), 22–30. https://doi.org/10.1016/j.micromeso.2009.07.025.

Rodríguez-Yáñez J. E. (2019). Parameters for Use of Waste Castor-Oil Seed (Ricinus Communis) as Biomass. *International Journal of Renewable Energy & Biofuels*, 2019, 1–8. https://doi.org/10.5171/2019.529157.

Sah M.K., Edbey K., EL-Hashani A., Almshety S., Mauro L., Alomar T.S., AlMasoud N., Bhattarai A. (2022) Exploring the Biosorption of Methylene Blue Dye onto Agricultural Products: A Critical Review. Separations, 9(9), 256. https://doi.org/10.3390/separations9090256

Saratale, R. G., Saratale, G. D., Chang, J. S., & Govindwar, S. P. (2011) Bacterial Decolorization and Degradation of Azo Dyes: A Review. *Journal of the Taiwan Institute of Chemical Engineers*, 42 (1), 138–57. https://doi.org/10.1016/j.jtice.2010.06.006.

Sherlala A. I. A., Raman A. A. A., Bello M. M. & Buthiyappan A. (2019) Adsorption of Arsenic Using Chitosan Magnetic Graphene Oxide Nanocomposite. *Journal of Environmental Management*, 246, 547–56. https://doi.org/10.1016/j.jenvman.2019.05.117.

Silva R.V.S., Gonçalves A.D., Vinhal J.O., Cassella R.J., Santos R.C., Dal Sasso M.A., Peixoto B.S., Borba-Santos L.P., Rozental S., Azevedo D.A., Romeiro G.A. (2021) Bioproducts from the pyrolysis of castor

seed cake: Basic dye adsorption capacity of biochar and antifungal activity of the aqueous phase, *Journal of Environmental Chemical Engineering*, 9(1) 104825, doi.org/10.1016/j.jece.2020.104825

Smahi, Zoubida. (2017). Essais de valorisation d'un déchet cellulosique : tiges de chardons dans l'élimination d'un colorant basique à partir de solutions aqueuses synthétiques. PhD thesis in Science, *Abou-Bekr Belkaïd–Tlemcen* University, Algeria.

Taimur S., Hassan M. I., Yasin T. (2017) Removal of Copper Using Novel Amidoxime Based Chelating Nanohybrid Adsorbent. *European Polymer Journal*, 95, 93–104. https://doi.org/10.1016/j.eurpolymj.2017.08.004.

Vakili, M., Deng, S., Cagnetta, G., Wang, W., Meng, P., Liu, D., & Yu, G. (2019). Regeneration of Chitosan-Based Adsorbents Used in Heavy Metal Adsorption: A Review. *Separation and Purification Technology*, 224, 373–87. https://doi.org/10.1016/j.seppur.2019.05.040.

Wong, Y. C., Szeto, Y. S., Cheung, W. H., & McKay, G. (2003). Equilibrium Studies for Acid Dye Adsorption onto Chitosan. *Langmuir* 19 (19), 7888–94. https://doi.org/10.1021/la030064y.

Xu, J., Xu, D., Zhu, B., Cheng, B., & Jiang, C. (2018). Adsorptive Removal of an Anionic Dye Congo Red by Flower-like Hierarchical Magnesium Oxide (MgO)-Graphene Oxide Composite Microspheres. *Applied Surface Science*, 435, 1136–42. https://doi.org/10.1016/j.apsusc.2017.11.232.

Zhi, L. L., & Zaini, M. A. A. (2017). Adsorption Properties of Cationic Rhodamine B Dye onto Metals Chloride-Activated Castor Bean Residue Carbons. *Water Science and Technology*, 75(4), 864–80. https://doi.org/10.2166/wst.2016.568.